

Supporting Information

for *Adv. Sci.*, DOI 10.1002/advs.202207497

Robust Spontaneous Raman Flow Cytometry for Single-Cell Metabolic Phenome Profiling via pDEP-DLD-RFC

Xixian Wang, Lihui Ren, Zhidian Diao, Yuehui He, Jiaping Zhang, Min Liu, Yuandong Li, Lijun Sun, Rongze Chen, Yuetong Ji, Jian Xu and Bo Ma**

Supporting Information

Robust spontaneous Raman flow cytometry for single-cell metabolic phenome profiling via pDEP-DLD-RFC

Xixian Wang, Lihui Ren, Zhidian Diao, Yuehui He, Jiaping Zhang, Min Liu, Yuandong Li, Lijun Sun, Rongze Chen, Yuetong Ji, Jian Xu, Bo Ma**

Figure S1. pDEP-DLD-RFC chip fabrication.

Figure S2. pDEP-DLD-RFC system operation.

Figure S3. Global IRCNs for the *NoDGAT2A*-expressing yeasts sampled at various time points from within the SCM or IM.

Figure S4. AXT content profiling for *H. pluvialis* under high light plus nitrogen depletion.

Figure S5. AXT content profiling for *H. pluvialis* under either high light or nitrogen depletion.

Figure S6. Ramanome-based profiling of TAG productivity in *NoDGAT2A*-expressing yeast.

Figure S7. Ramanome-based degree of lipid unsaturation (DU) profiling in *NoDGAT2A*-expressing yeast.

Figure S8. Ramanome-based CD Ratio (CDR) profiling in yeast.

Figure S9. Global IRCNs for *NoDGAT2A*-expressing yeast that were supplemented with D₂O following various temporal incubations in induction medium.

Figure S10. Global IRCNs for four cancer cell lines: T24 (bladder), A549 (lung), OSRC-2 (renal) and MCF-7 (breast).

Movie S1. pDEP-DLD based cell focusing.

Movie S2. Single-cell trapping and release after pDEP-DLD based cell focusing.

Supplementary Figures

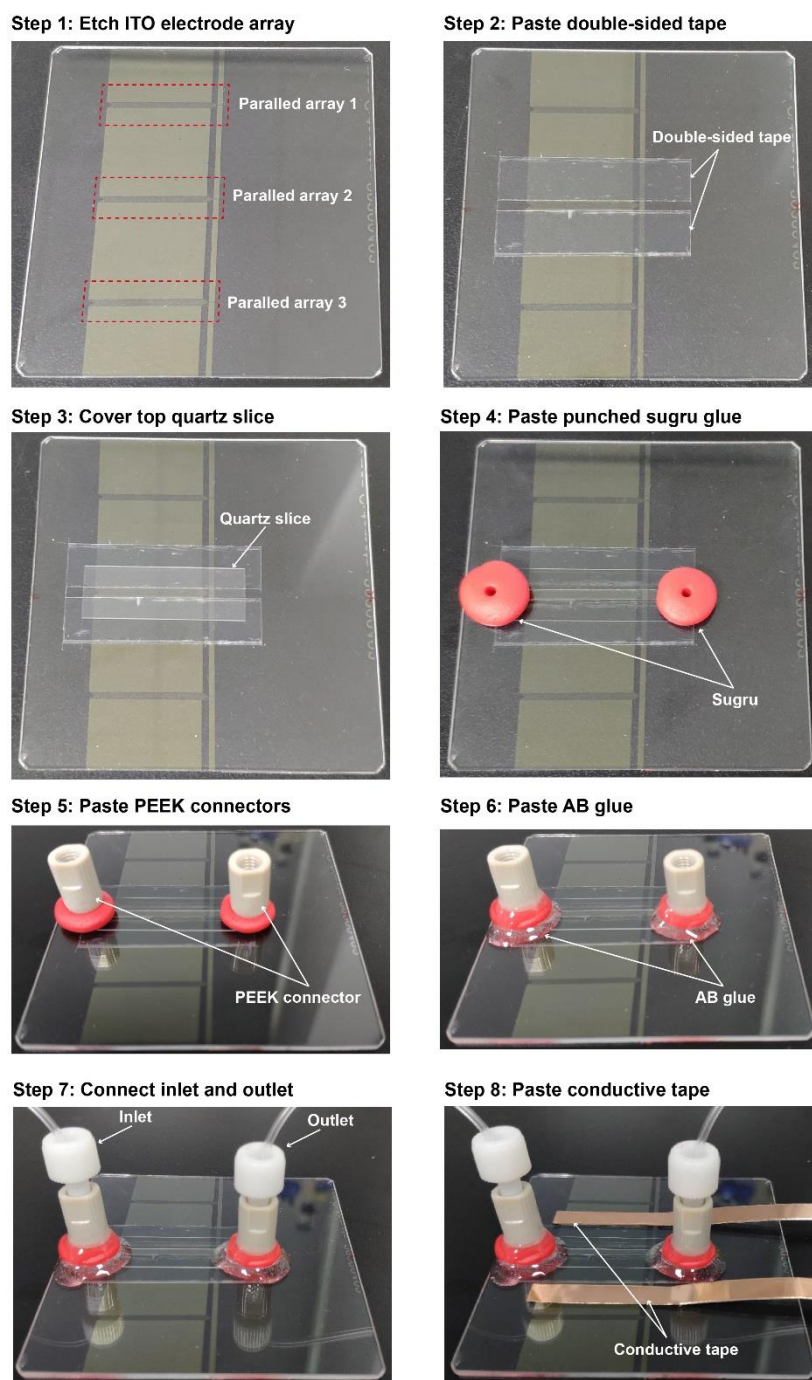


Figure S1. pDEP-DLD-RFC chip fabrication. **Step 1:** etching the ITO electrode array; **Step 2:** pasting the double-sided tape to construct the loading channel; **Step 3:** covering the top quartz slice to facilitate SCRS acquisition; **Step 4:** applying the punched sugru glue to connect the PEEK connector; **Step 5:** placing the PEEK connector on sugru glue; **Step 6:** applying the AB glue to immobilize the PEEK connector; **Step 7:** connecting the inlet and outlet for loading and exporting cells; **Step 8:** conductive tape placement for the pDEP.

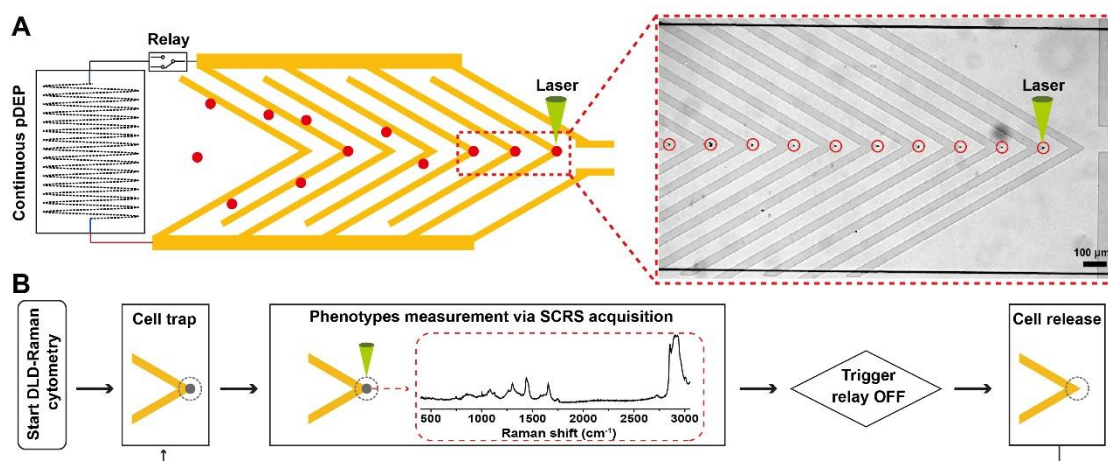


Figure S2. pDEP-DLD-RFC system operation. (A) Operation strategy to enable high throughput SCRS profiling. Fast-moving single cells are focused by pDEP-DLD and delivered to the Raman laser by repeated trap-releases. An inset bright-field image displays single cells that are trapped and released (a still extracted from Movie S2). (B) QSpec software workflow for efficient SCRS acquisition. Scale bar, 100 μm .

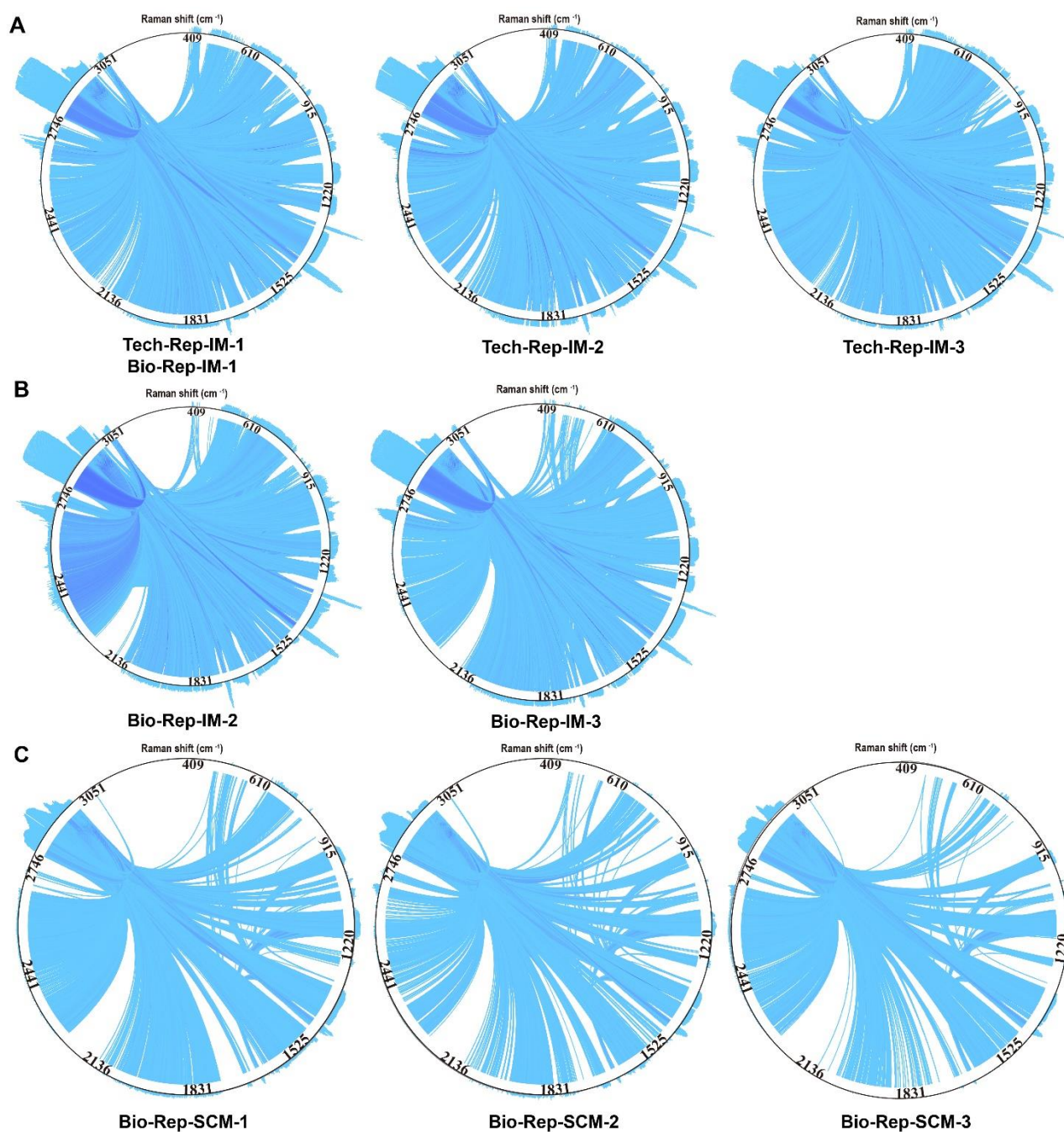


Figure S3. Global IRCNs for the *NoDGAT2A*-expressing yeasts sampled at various time points from within the SCM or IM. IM IRCNs for the (A) technical replicates, (B) biological replicates. (C) IRCNs for the Biological replicates in SCM.

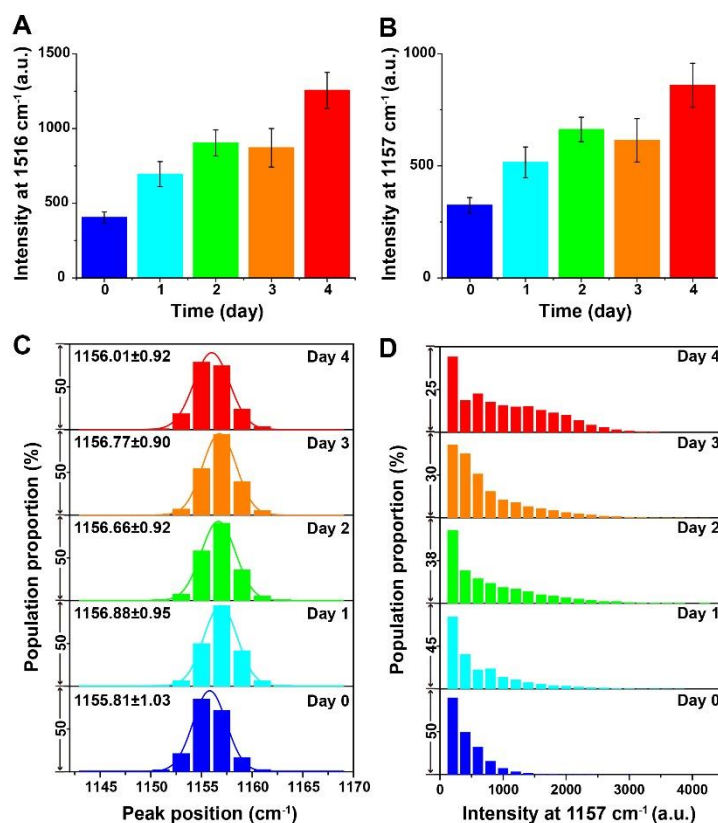


Figure S4. AXT content profiling for *H. pluvialis* under high light plus nitrogen depletion. Average Raman intensity at (A) 1516 cm⁻¹ and (B) 1157 cm⁻¹. Error bars: SD of three replicates. (C) Distribution around the 1157 cm⁻¹ peak during the four-day cultivation. (D) Temporal tracking of AXT-production by *H. pluvialis* cells during the four-day cultivation. Error bars indicate the SD of three independent experiments.

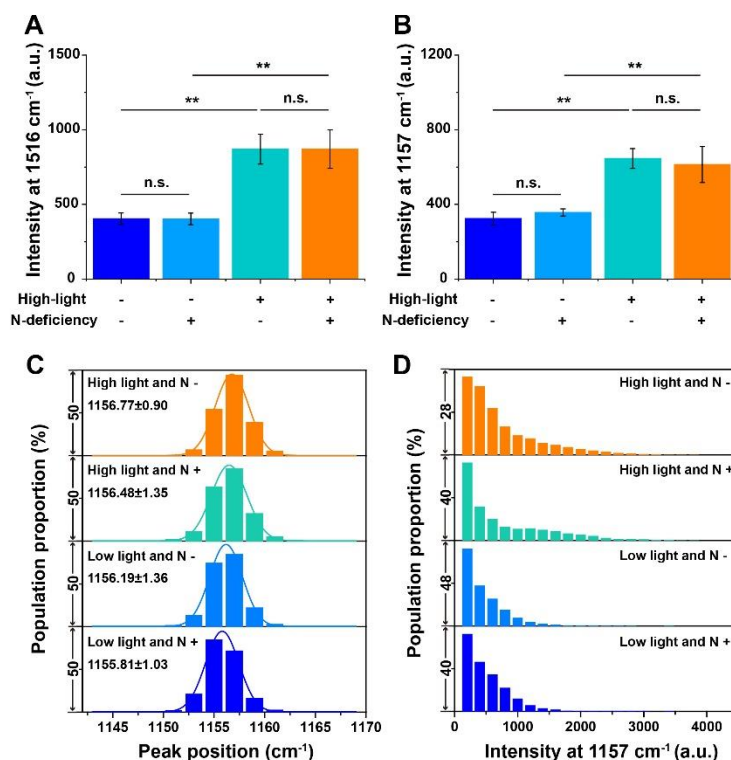


Figure S5. AXT content profiling for *H. pluvialis* under either high light or nitrogen depletion. Average Raman intensity at (A) 1516 cm⁻¹ and (B) 1157 cm⁻¹ under different stress conditions. Error bars: SD of three replicates. ** $P < 0.01$; n.s., not significant. (C) Distribution around the 1157 cm⁻¹ peak under different stress conditions. (D) Comparison of AXT-production by *H. pluvialis* cells with various stress conditions. Error bars indicate the SD of three independent experiments. The statistic difference in (A) and (B) was analyzed using the unpaired two-tailed Student's *t*-test.

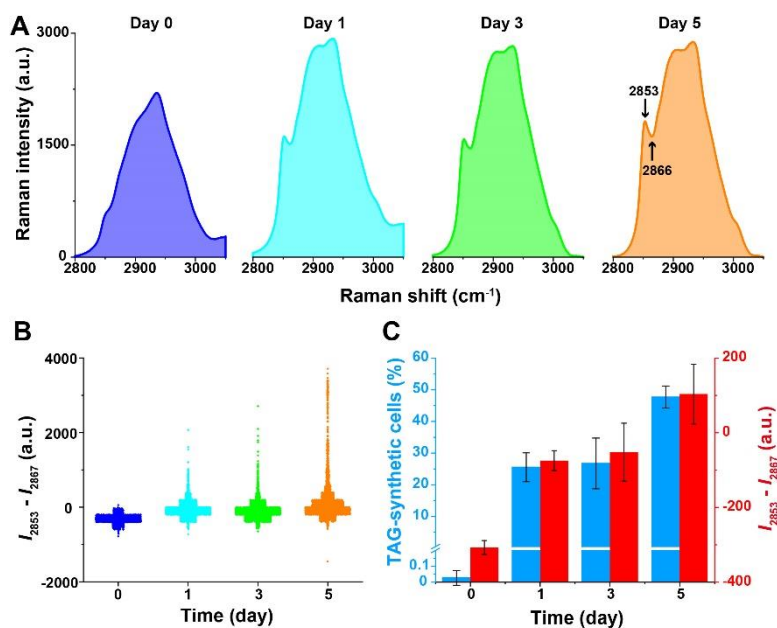


Figure S6. Ramanome-based profiling of TAG productivity in *NoDGAT2A*-expressing yeast. (A) The average SCRS at 2800 to 3050 cm⁻¹ ($n > 3500$) for *NoDGAT2A*-expressing yeast cells, showing a gradual TAG production increase over the induction time. (B) Distribution of “ $I_{2853} - I_{2867}$ ” (representing TAG content). (C) Percentage of TAG-synthetic cells (blue/left, showing those $I_{2853} - I_{2866} > 0$) and average “ $I_{2853} - I_{2866}$ ” (red/right). Error bars indicate the SD of three independent experiments.

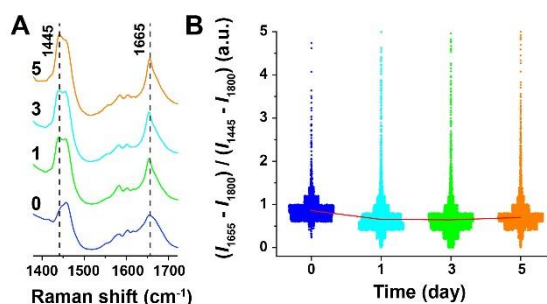


Figure S7. Ramanome-based degree of lipid unsaturation (DU) profiling in *NoDGAT2A*-expressing yeast. (A) The average SCRS at 1400 to 1700 cm^{-1} ($n > 3500$) for *NoDGAT2A*-expressing yeast cells. (B) Distribution around “ $(I_{1665} - I_{1800}) / (I_{1445} - I_{1800})$ ” (representing DU).

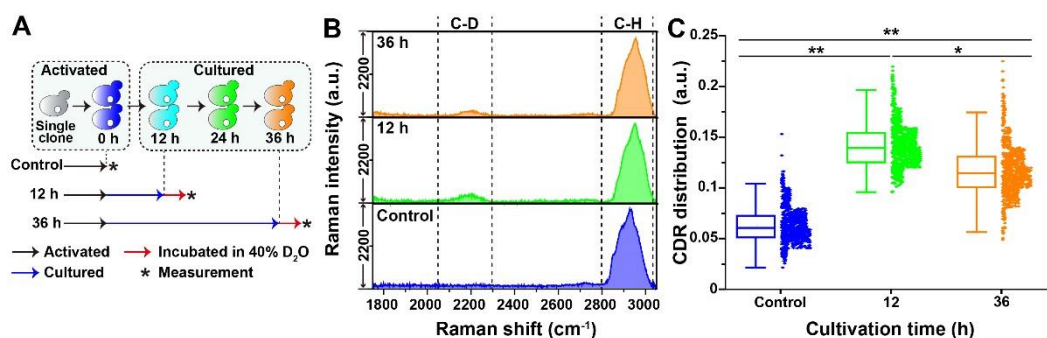


Figure S8. Ramanome-based CD Ratio (CDR) profiling in yeast. (A) Yeast preparation with different culture durations and incubated with D_2O under identical conditions. (B) The average SCRS at 1800 to 3000 cm^{-1} ($n > 3500$) incubated with D_2O . (C) CDR distribution (representing metabolic activity). The lines in the box indicate the mean value. * $P < 0.05$; ** $P < 0.01$. The statistic difference in (C) was analyzed using the unpaired two-tailed Student t-test.

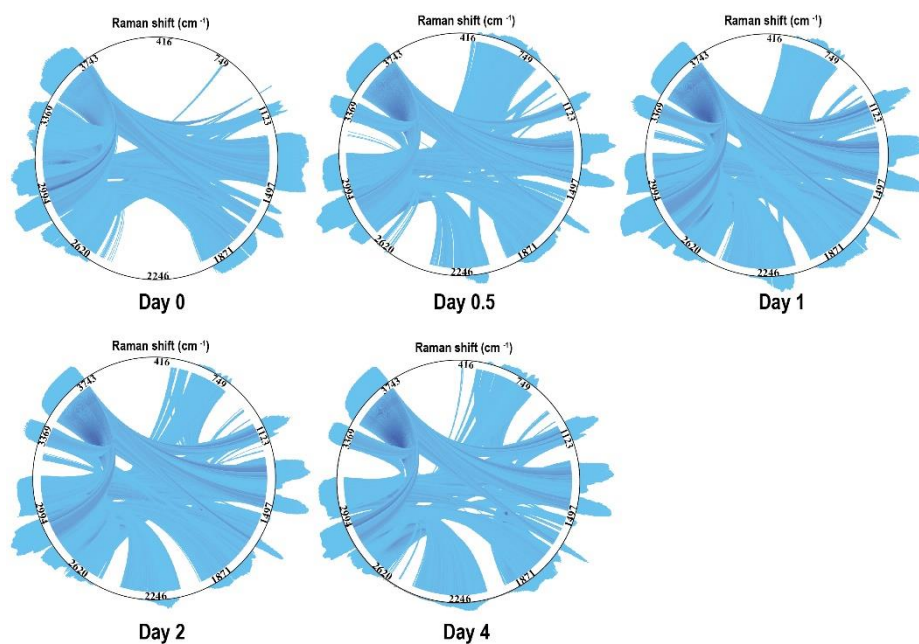


Figure S9. Global IRCNs for *NoDGAT2A*-expressing yeast that were supplemented with D_2O following various temporal incubations in induction medium. IRCNs derived from the yeast ramanomes.

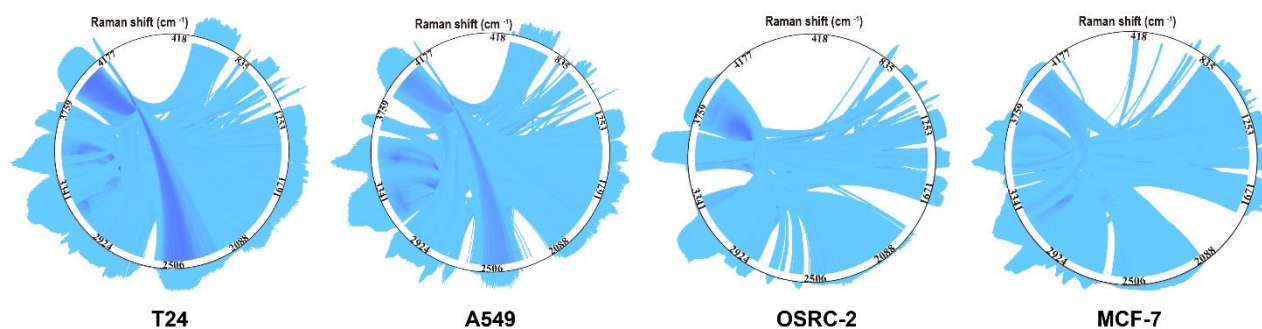


Figure S10. Global IRCNs for four cancer cell lines: T24 (bladder), A549 (lung), OSRC-2 (renal) and MCF-7 (breast). IRCNs derived from cancer ramanomes.